Applied Catalysis B: Environmental 205 (2017) 93–103

Contents lists available at ScienceDirect

Applied Catalysis B: Environmental

journal homepage: www.elsevier.com/locate/apcatb

Comparison of citric acid and glycol effects on the state of active phase species and catalytic properties of CoPMo/Al_2O_3 hydrotreating catalysts

Aleksey Pimerzin[a], Alexander Mozhaev[a], Andrey Varakin[a], Konstantin Maslakov[b], Pavel Nikulshin[a,*]

[a] Samara State Technical University, 244 Molodogvardeiskaya St., Samara 443100, Russia
[b] Department of Chemistry, Lomonosov Moscow State University, Leninskie Gory, Moscow 119991, Russia

ARTICLE INFO

Article history:
Received 16 October 2016
Received in revised form
30 November 2016
Accepted 7 December 2016
Available online 8 December 2016

Keywords:
Hydrotreating
Heteropolyanion
CoMoS
Citric acid
Triethylene glycol

ABSTRACT

CoPMo/Al_2O_3 catalysts were prepared using $H_3PMo_{12}O_{40}$ and Co complexes with citric acid (CA) or non-complexing organic additives such as ethylene glycol (EG), diethylene glycol, triethylene glycol (TEG), glycerol, and a mixture of EG and CA. The catalysts were characterized by low-temperature N_2 adsorption, Raman spectroscopy, thermogravimetric analysis, temperature-programmed reduction, X-ray photoelectron spectroscopy, and high-resolution transmission electron microscopy. The prepared samples were tested in hydrodesulfurization (HDS) of dibenzothiophene (DBT). The addition of either CA or glycols led to several beneficial effects such as weakening of the slab-support interaction at enhancing the promotion degree, dispersion and stacking number of the CoMoS species. It has been shown that the promotion degree of CoMoS edges increased with a pore volume gain by the additive-impregnated catalysts after their sulfidation. Catalysts with CA, TEG or the EG-CA mixture demonstrated higher activity in DBT HDS. Probable reasons for the found relationships are discussed.

1. Introduction

Manufacture of clean fuels has been so far one of the most challenging issues in a modern oil refinery. Varying feedstock quality and unconventional hydrocarbon resources involved in hydroprocessing call for more active hydrotreating (HDT) catalysts to enhance optimization and energy efficiency of hydroprocessing. Hydrodesulfurization (HDS) of petroleum feedstock is generally performed with Co(Ni)Mo/Al_2O_3 catalysts, in which the Co(Ni)MoS active phase consists of nanosized MoS_2 slabs decorated with Co(Ni) atoms [1]. Active catalysts are obtained by sulfidation of a supported oxidic precursor. The latter is typically prepared by the incipient wetness impregnation of γ-Al_2O_3 with an aqueous solution containing Co and Mo, followed by a drying and a calcination step [2,3]. The catalyst preparation is a key step to reach high activities and to avoid any loss of cobalt atoms to inactive species like $CoAl_2O_4$ and bulk CoS_x.

During the last decade, many improvements have been made to increase the active phase portion in Co(Ni)Mo/Al_2O_3 catalysts. Heteropolyanions (HPAs) as precursors offer new opportunities for improving catalysts' activity [4]. Various types of HPAs with Keggin $[XM_{12}O_{40}]^{n-}$ and lacunary Keggin $[XM_{9-11}O_{34-39}]^{n-}$ [5–15], Anderson $[XM_6O_{24}H_6]^{n-}$ [16–31], Strandberg $[X_2M_5O_{23}{}^{n-}]$ or Waugh $[Ni_9MoO_{32}]^{6-}$ structures [32,33] (where M(M') is a metallic cation and X a non-metallic one) have been reported. These generally let afford better catalytic performance than their counterparts based on conventional precursors due to improved sulfidation allowed by a better dispersion of the oxidic precursor even at high metallic loadings [4]. Cobalt salt of the dimer of Anderson-type HPA $Co_2Mo_{10}O_{39}H_4{}^{6-}$ is an interesting starting material to introduce both metals into the same entity, without foreign counterions and with a Co/Mo ratio equal to 0.5 corresponding to the optimum Co/Mo ratio for conventional HDT catalysts [16,23,34,35]. The association of Co and Mo at the molecular level in the same HPA preserved after drying of the catalyst ensured efficiency for the promoting effect with a larger CoMoS active phase. This HPA-based system was further improved by a simultaneous use of Co_2Mo_{10}HPA and chelating agents [36–38]. Also, the simultaneous use of Keggin HPA and Co(Ni)-chelates for preparation of HDT catalysts was investigated in a few other works [39–42]. The CoMoS active phase species were formed more selectively when Co_2Mo_{10}HPA and Co–chelate complexes simultaneously used for

* Corresponding author.
E-mail address: p.a.nikulshin@gmail.com (P. Nikulshin).

http://dx.doi.org/10.1016/j.apcatb.2016.12.022
0926-3373/

Table 1
Composition and textural properties of prepared Co-Add-PMo catalysts in oxide and sulfided states.

Catalyst	Atomic ratio Co/Mo	Content in the catalyst (wt.%)			Textural characteristics of oxide (sulfided) samples			Pore volume distribution for oxide (sulfided) samples (%)			
		Mo	Co	Carbon	Specific surface area (m^2/g)	Pore volume (cm^3/g)	Average pore diameter (Å)	<40 Å	40–80 Å	80–170 Å	>170 Å
Alumina	–	–	–	–	187	0.57	80	0	54	44	3
Co-PMo	0.50	12.0	3.7	0.2	149 (127)	0.25 (0.32)	104 (64)	4 (6)	29 (51)	64 (35)	3 (8)
Co-CA-PMo	0.49	12	3.6	1.8	132 (277)	0.14 (0.30)	102 (38)	6 (24)	27 (32)	61 (35)	6 (9)
Co-EG-PMo	0.50	12	3.7	0.6	74 (156)	0.23 (0.26)	104 (64)	0 (7)	31 (45)	66 (39)	3 (8)
Co-DEG-PMo	0.49	12	3.7	1.1	78 (171)	0.24 (0.33)	102 (64)	0 (9)	35 (38)	60 (44)	4 (9)
Co-TEG-PMo	0.50	12	3.6	1.4	56 (203)	0.18 (0.34)	102 (48)	5 (15)	32 (50)	58 (28)	4 (7)
Co-Gly-PMo	0.51	12	3.7	0.9	57 (214)	0.19 (0.33)	102 (64)	0 (8)	29 (40)	67 (45)	4 (8)
Co-EG-CA-PMo	0.51	12	3.7	2.5	25 (276)	0.09 (0.28)	104 (38)	0 (31)	22 (33)	70 (30)	7 (6)

catalyst preparation [37]. It was attributed to delaying sulfidation of promoter atoms at low temperature due to formation of stable complexes with chelating agents. However, the Co–chelate addition significantly changed the active phase morphology due to different interactions between precursors and support surfaces in each catalyst. Citric acid (CA)- and tartaric acid-containing catalysts showed higher activity than the nitrilotriacetic acid- and ethylenediaminetetraacetic acid-containing counterparts. It was shown that high catalytic performance was more directly related to the (Co/Mo) ratio at the edge of MoS_2 slabs. More recently, we reported [38] that loading of Co and Mo from Co_2Mo_{10}HPA and Ni from nickel-citrate led to formation of ternary NiCoMoS/Al_2O_3 catalysts with enhanced performance as compared to CoMoS/Al_2O_3 analogs. It was achieved due to the co-promotion effect of both metals and probably due to sequential sulfidation of Co_2Mo_{10}HPA and Ni-citrate precursors with formation of the NiCoMoS phase having CoMoS and NiMoS active sites or mixed NiCoMoS sites that are readily accessible by the reactants.

Not long ago, Costa et al. [36] investigated the use of additive-impregnated dried catalysts on a series of various CoMo/Al_2O_3 solids prepared by the conventional route, $Co_2Mo_{10}Co$, and a solution containing $P_2Mo_5O_{23}^{6-}$ and Co^{2+} (Co/Mo = 4). The additive impregnation step was performed on the dried solid by the incipient wetness impregnation with an aqueous solution of triethylene glycol (TEG) with a TEG/Mo molar ratio close to 0.75. It was reported that formation of the "CoMoS" phase was needed but not sufficient to explain catalytic performance of all studied catalysts. Catalytic activity in toluene hydrogenation of additive-free dried, additive-impregnated dried and calcined catalysts directly correlates with the number of mixed Co–Mo sites present at the MoS_2 edges. Using TEM, XPS and DFT calculations the authors concluded that the organic additive was used to produce a higher number of mixed Co-Mo sites rather than to create different active sites.

The aim of the research was to compare effects of CA as a chelating agent and of glycols as non-complexing organic additives on the state of active phase species and catalytic properties of CoPMo/Al_2O_3 HDT catalysts prepared with Keggin-type $H_3PMo_{12}O_{40}$ HPA frequently used as an alternative to classical ammonium heptamolybdate.

2. Experimental

2.1. Preparation of Co-Add-PMo catalysts

Co-Add-PMo catalysts were prepared by the incipient wetness technique via the impregnation of γ-Al_2O_3 (Engelhard) of 0.25–0.5 mm with acidic aqueous solutions (pH ≈ 3–4) containing the required amounts of 12-molybdophosphoric heteropolyacid $H_3PMo_{12}O_{40} \times 3H_2O$, $Co(CH_3COO)_2{\cdot}4H_2O$ or $CoCO_3$ (Aldrich) and organic additives with molar ratios Add/Mo = 1/1 and Co/Mo = 0.5. CA, ethylene glycol (denoted as EG), diethylene glycol (denoted as DEG), TEG, glycerol (denoted as Gly), and the EG – CA mixture with the equal molar ratio were purchased in Aldrich and were used as organic additives for catalyst preparation. All impregnated solids were aged at room temperature overnight and subsequently air-dried at 110 °C for 10 h without calcination. The content of Mo and Co in the catalysts was measured using an EDX800HS analyzer (Table 1).

To analyze the catalysts in the active state, the obtained oxidic samples were sulfided. A mixture of dimethyldisulfide (DMDS, 2 wt% of sulfur) and decane at 3.5 MPa was utilized in a stepwise procedure conducted over 10 h at 240 °C and 8 h at 340 °C.

2.2. Characterization of the catalysts

2.2.1. Textural characteristics

The textural characteristics of the prepared catalysts were measured by low-temperature N_2 adsorption on a Quantachrome Autosorb-1 porosimeter. Before the adsorption measurement, the sulfided samples were outgassed under vacuum (<10^{-1} Pa) at 350 °C for 4 h. Specific surface area (SSA) was calculated using the BET method. The total pore volume and pore size distribution were found from a desorption branch of the isotherm using the BJH model.

2.2.2. Raman spectroscopy

The Raman spectra of the samples were recorded using a Senterra (Bruker) laser Raman spectrometer (λ = 532 nm) at room temperature. The spectra were recorded from 100 to 3300 cm^{-1} with an accuracy of 2 cm^{-1}. However, due to the intense background signal of alumina supports, only the 200–1100 cm^{-1} spectral range characteristic of the Mo—O stretching vibrational mode is presented.

2.2.3. Thermogravimetric analysis

Simultaneous differential scanning calorimetry (DSC) and thermogravimetric analysis (TGA) of the oxide Co-Add-PMo catalysts were carried out using a NETZSCH STA 4449 F3 Jupiter apparatus. TGA-DSC curves were recorded in flowing air in the range from room temperature to 600 °C (heating rate 10 °C/min). For analysis, 20 mg of a sample was loaded in a corundum crucible; calcined alumina was used as a reference sample.

2.2.4. Temperature-programmed reduction (TPR)

The TPR analysis of the catalysts in oxide and sulfide states was carried out using a thermal conductivity detector (TCD). For analyzing the catalysts in oxide state, the samples were calcined at 400 °C for 4 h to remove Add and water, hindering TPR measurements. For analyzing the catalysts in sulfide state, the dried samples were sulfided in a quartz reactor at 400 °C for 4 h with a mixture of H_2S and H_2 (10 vol.% of H_2S), heating rate 5 °C/min, then cooled to room temperature and passed over to the TPR analysis without a contact

of air. The analysis was held in a mixture of H_2 and N_2 (5 vol.% of H_2) under the following conditions: the gas flow rate 30 ml/min, temperature range from 20 to 900 °C with a holding period at 900 °C for 1 h, and heating rate 10 °C/min.

2.2.5. X-ray photoelectron spectroscopy (XPS)

The sulfided catalysts were analyzed by XPS in order to identify chemical species on the surface using a Kratos Axis Ultra DLD spectrometer with a monochromatic AlK_a source (hn = 1486.6 eV, 150 W). The binding energy (BE) scale of the spectrometer was pre-calibrated using peak positions for Au $4f_{7/2}$ (83.96 eV) and Cu $2p_{3/2}$ (932.62 eV) core levels of pure metallic gold and copper. Individual high resolution spectral regions were determined to obtain BE of the peaks, assign the chemical state of the elements, and calculate relative ratios of the elements on the catalyst surface. The spectra were analyzed using the CasaXPS processing software after applying a Shirley background subtraction. Gaussian (30%)–Lorentzian (70%) peaks were used for the spectra deconvolution. Decompositions of the S 2p, Mo 3d, and Co 2p XPS spectra were performed according to [37,38] using appropriate supported monometallic catalysts as oxidic and sulfided References

Atomic concentrations of each element for every sulfided catalyst and relative concentrations of each species, cobalt oxide Co^{2+}, CoS_x, CoMoS, molybdenum oxide Mo^{6+}, MoS_xO_y and MoS_2 for every sulfided catalyst were determined. For example, the relative CoMoS amount was evaluated using the following equation:

$$[\mathrm{CoMoS}](\%) = \frac{A_{\mathrm{CoMoS}}}{A_{\mathrm{CoMoS}} + A_{\mathrm{CoS_X}} + A_{\mathrm{Co^{2+}}}} \times 100, \quad (1)$$

where A_X represents the peak area of species x.

The effective Co content (wt.%) in the CoMoS phase was determined as follows:

$$C_{\mathrm{CoMoS}} = [\mathrm{CoMoS}] \times C(\mathrm{Co})_{\mathrm{T}}, \quad (2)$$

where $C(Co)_T$ represents the effective concentration of cobalt on the catalyst surface found by XPS (wt.%).

The promoter ratio in the CoMoS phase slab was calculated using the following relations:

$$\left(\frac{\mathrm{Co}}{\mathrm{Mo}}\right)_{\mathrm{slab}} = \frac{C_{\mathrm{CoMoS}}}{C_{\mathrm{MoS_2}}}, \quad (3)$$

where C_{CoMoS} and C_{MoS_2} are absolute concentrations of Co and Mo in the CoMoS and MoS_2 species, respectively (at%).

The promoter ratio in the slab edge of the active phase was calculated as follows:

$$\left(\frac{\mathrm{Co}}{\mathrm{Mo}}\right)_{\mathrm{edge}} = \frac{(\mathrm{Co/Mo})_{\mathrm{slab}}}{D}, \quad (4)$$

where D is the dispersion of active phase particles obtained using TEM measurements.

The absence of any signal at 169.0 eV (characteristic of sulfates) indicated that sulfided catalysts were not reoxidised during the transfer of the sample from the sulfiding reactor to the XPS chamber.

2.2.6. High-resolution transmission electron microscopy (HRTEM)

HRTEM images of the sulfided catalysts were taken on a Tecnai G2 20 electron microscope in the high-resolution mode with the accelerating voltage of 200 kV and lattice-fringe resolution of 0.14 nm. Preparation of the samples included their application on a perforated carbon film and further imposition on a copper grid. About 10–15 representative micrographs were visually inspected for each catalyst. To measure the key morphological characteristics at least 500 slabs were handled for every sample.

The average slab length of CoMoS slabs was calculated as follows:

$$\overline{L} = \frac{\sum_{i=1..t} l_i}{n}, \quad (5)$$

where l_i is the length of slab i, n is the total number of slabs.

The average number of slabs per stack ($\overline{N}$) was calculated as follows:

$$\overline{N} = \frac{\sum_{i=1..t} n_i N_i}{\sum_{i=1..t} n_i}, \quad (6)$$

where n_i is the number of stacks in N_i layers.

To measure the extent of the CoMoS dispersion, the average fraction of Mo atoms at the MoS_2 edge surface was calculated, assuming that the MoS_2 slabs were perfect hexagons [43,44]. The MoS_2 dispersion (D) was statistically evaluated by dividing the total number of Mo atoms at the edge surface (Mo_e), including corner sites (Mo_c), by the total number of Mo atoms (Mo_T) using the slab sizes measured from the TEM micrographs:

$$D = \frac{Mo_e + Mo_c}{Mo_T} = \frac{\sum_{i=1..t} 6n_i - 6}{\sum_{i=1..t} 3n_i^2 - 3n_i + 1}, \quad (7)$$

where n_i is the number of Mo atoms along one side of the MoS_2 slab, as determined by its average slab length $\overline{L}$ (nm), and t is the total number of slabs in the TEM micrographs.

2.3. Examination of the catalytic properties

The catalytic properties were determined using a fixed-bed microreactor featuring a high-pressure flow system. A 0.15 g sample of the catalyst (0.25–0.50 mm) was diluted with 1 cm^3 of low-surface-area carborundum (0.2–0.4 mm) and placed in the centre of the reactor (with an internal diameter 0.8 cm). Before testing, the catalysts were sulfided with a mixture of decane spiked with DMDS (2 wt.% of sulfur) at 3.5 MPa in a stepwise procedure over 10 h at 240 °C and 8 h at 340 °C. A mixture of DBT (1500 ppm S), hexadecane (as an internal standard, 1 wt.%) and toluene (as a solvent) was used as a model feedstock for evaluating HDS performance. Catalysts were tested under the following conditions: 250 °C, 3.0 MPa hydrogen, 40 and 80 h^{-1} liquid hourly space velocity (LHSV) and a 500 NL/L volume ratio of H_2 to feed. Liquid product compositions of the samples collected every 0.5 h were determined using a Crystall-5000 Gas Chromatograph equipped with a 30 m OV-101 column. The reaction products were identified by GC/MS analysis using a Finnigan Trace DSQ. The HDS reaction was allowed to proceed for 10 h to achieve a steady state of the catalyst.

The rate constant of the pseudo-first-order of DBT HDS was determined using the following equation:

$$k_{\mathrm{HDS}} = -\frac{F_{\mathrm{DBT}}}{W} \ln(1 - x_{\mathrm{DBT}}), \quad (8)$$

where k_{HDS} is the pseudo-first-order reaction constant for DBT HDS (mol g^{-1} h^{-1}); x_{DBT} is the conversion (%) of DBT; F_{DBT} is the reactant flow (mol h^{-1}) and W is weight of the sulfided catalyst (g).

The HDS products from DBT included biphenyl (BP) via the direct desulfurization (DDS) pathway, as well as cyclohexylbenzene (CHB) and bicyclohexyl (BCH) from the HYD pathway. Only traces of hydrogenated tetrahydro- and perhydrodibenzothiophenes were

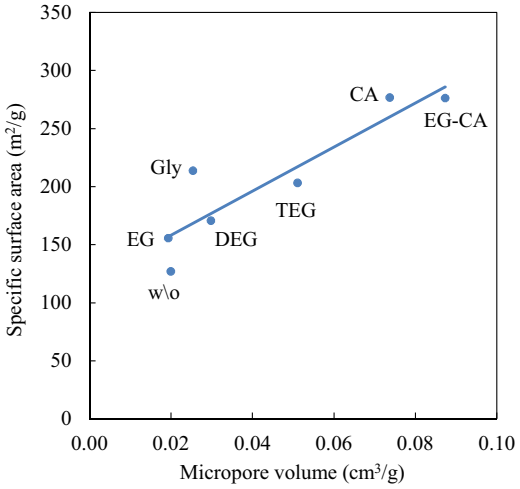

Fig. 1. Micropore volume vs SSA of sulfided Co-Add-PMo catalysts.

observed. The HYD/DDS selectivity was calculated according to the reaction network for DBT HDS:

$$S_{HYD/DDS} = \frac{k_{HYD}}{k_{DDS}} = \frac{C_{CHB} + C_{BCH}}{C_{BP}}, \quad (9)$$

where C_{CHB}, C_{BCH} and C_{BP} are concentrations (mol.%) of CHB, BCH and BP in the reaction products, respectively.

In order to explain changes in activities of the catalysts depending on the composition and characteristics of the species of the CoMoS active phase, turnover frequencies (TOF, s^{-1}) normalized on edge sites of the CoMoS slabs for HDS of DBT were calculated as follows:

$$TOF_{HDS} = \frac{F_{DBT} \cdot x_{DBT} \cdot Mr_{Mo}}{W \cdot C_{MoS_2} \cdot D \cdot 3600}, \quad (10)$$

where F_{DBT} is the DBT flow (mol h^{-1}); x_{DBT} is the conversion at low contact time (%) of DBT; W is weight of the catalyst (g); C_{MoS_2} is the effective Mo content in the MoS_2 or CoMoS species (wt.%); D is the dispersion of the MoS_2 or CoMoS species and Mr_{Mo} is the molar mass of molybdenum (95.9 g/mol).

3. Results and discussion

3.1. Characteristics of catalysts in the oxidic state

3.1.1. Textural properties

The prepared Co-Add-PMo catalysts had a close content of Mo and Co though different in the carbon amount in the sulfided solids (Table 1) and in the textural characteristics in both oxidic and sulfided states. The specific surface area (SSA) and pore volume decreased after precursors loading to the support and drying of all catalysts. However, the obtained oxide samples significantly differed in their SSA and pore volume. The Co-EG-CA-PMo sample had the lowest SSA equal to 25 m^2/g that witnessed to almost full filling of the catalyst pores with oxidic precursors and polycondensate formed by EG and CA molecules. In contrast, the Co-PMo and Co-CA-PMo samples had 149 and 132 m^2/g of SSA, respectively. The average pore size and pore size distribution for oxidic Co-Add-PMo catalysts were approximately equal for all samples. Textural properties of the catalysts were measured repetitively after their sulfidation. It appeared that, during the catalyst activation, SSA and pore volume values increased 2–11-fold. Moreover, the Co-CA-PMo, Co-TEG-PMo, Co-Gly-PMo and Co-EG-CA-PMo catalysts had higher SSA values than the initial support. It was possible due to formation of a secondary coke-connected pore structure. The

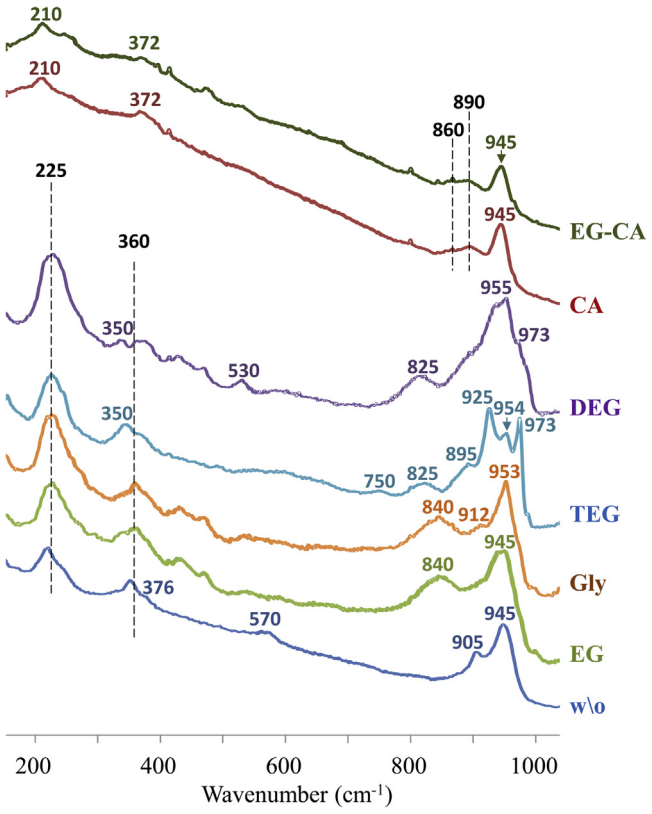

Fig. 2. Raman spectra of oxide Co-Add-PMo catalysts dried at 110 °C.

sulfided Co-Add-PMo catalysts had a diverse pore size distribution and the average pore diameter varied from 38 to 64 Å. The lower average pore diameter corresponded to the samples having a higher coke content (1.4-2.5 wt%) after sulfidation and most part of micropore volume (Table 1). As earlier reported [37,42,45], the existence of secondary pores with the ca. 38 Å diameter in chelating agent-based catalysts corresponds to coke species formed on the alumina surface. SSA of the sulfided samples well correlated with their micropore volume (Fig. 1). Therefore, extra-high SSA values of the mentioned catalysts were due to formation of the carbon-contained species with the advanced pore structure inside the pores of the alumina support.

3.1.2. Raman spectroscopy

Fig. 2 shows the Raman spectra of dried Co-Add-PMo catalysts. The reference sample without any additives exhibited bands at 945, 905, 360 and 225 cm^{-1}. These bands are typical for $[H_xMo_7O_{24}]^{(6-x)-}$ [46,47]. The band at 376 cm^{-1} indicated the presence of $[H_xP_2Mo_5O_{23}]^{(6-x)-}$ anions on the catalyst surface. Their other main bands are located around 940, 890, 395 and 210 cm^{-1} [48]. Therefore, the bands detected at 939, 900 and 213 cm^{-1} originate from the superposition effect between the $[H_xMo_7O_{24}]^{(6-x)-}$ and $[H_xP_2Mo_5O_{23}]^{(6-x)-}$ species. Of note is the absence of specific bands of other possible P-containing HPAs with Keggin $[PMo_{12}O_{40}]^{3-}$ or $[H_2PMo_{11}CoO_{40}]^{5-}$, lacunary $[PMo_{11}O_{39}]^{7-}$, $[PMo_9O_{31}]^{3-}$ or $[PMo_{10}O_{34}]^{3-}$ and Dawson $[P_2Mo_{18}O_{62}]^{6-}$ structures showing ν(Mo=O) bands above 970 cm^{-1} [7–9,48]. Moreover, the small broad band at 570 cm^{-1} corresponds to ν(X—O—Mo) stretching vibrations of Anderson HPAs $[XM_6O_{24}H_6]^{n-}$ with X of Al and/or Co [49].

After the CA addition to the impregnation solution, the Raman bands of Anderson HPAs at 530–570 cm^{-1} (the exact position of the band depends on the nature of heteroatom X and of the counter-cation) disappeared. The Raman spectra of the Co-CA-PMo and

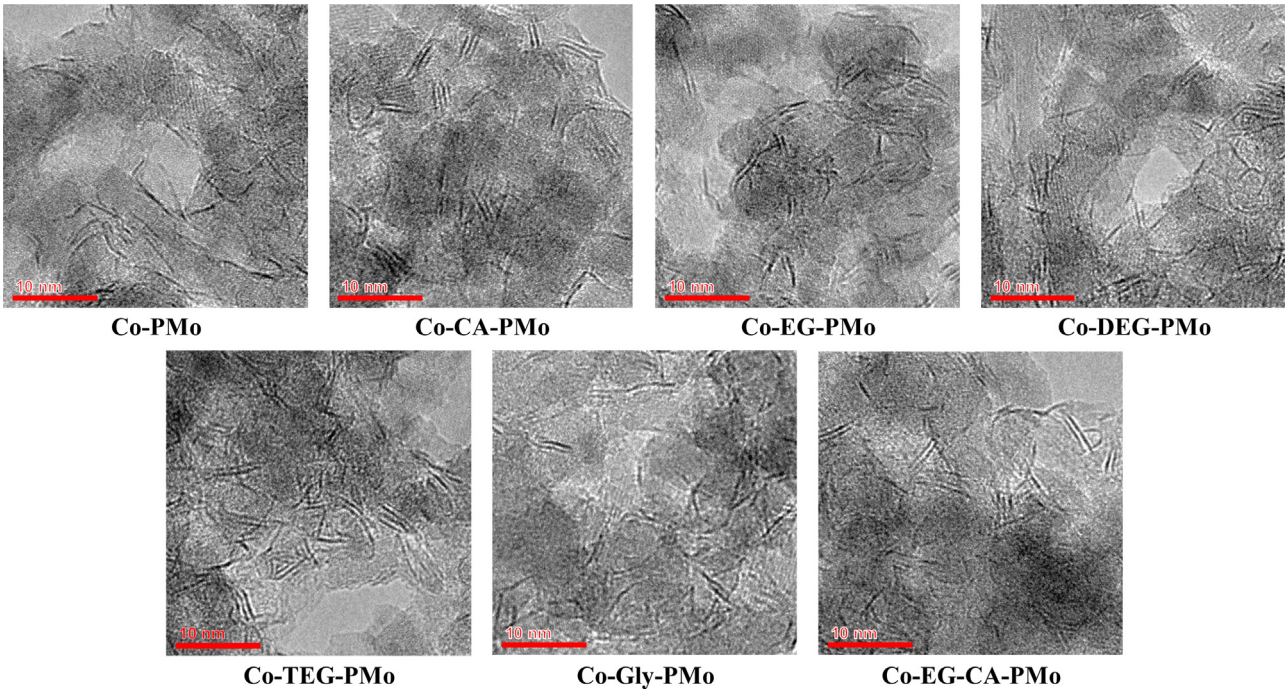

Fig. 3. HRTEM micrographs of sulfided Co-Add-PMo catalysts.

Co-EG-CA-PMo catalysts exhibited two major peaks at 945 and 890 cm^{-1}, a shoulder at 860 cm^{-1}, and the small bands at 372 and 210 cm^{-1}, which are characteristic of the $[Mo_4O_{11}(C_6H_5O_7)_2]^{4-}$ complex existing inside the Al_2O_3 pores [50]. No free CA seems to be present considering the Raman peak absence at 785 cm^{-1}; however, one cannot rule out a strong citrate-Al_2O_3 interaction.

For the Co-EG-PMo catalyst, no significant modification of its Raman spectrum was observed, except a few bands at about 840 cm^{-1}, arising from ν_{as}(Mo═O) stretching vibrations in $[MoO_4]^{2-}$ and ν(C—O) of EG [46]. The Raman spectrum of the Co-Gly-PMo catalyst exhibited main bands at 953 and 840 cm^{-1} that corresponded to the existence of both $[P_2Mo_5O_{23}]^{6-}$ and $[MoO_4]^{2-}$ particles.

Using of TEG and DEG in the impregnation solution led to formation of a greater amount of the $[P_2Mo_5O_{23}]^{6-}$ species with corresponding bands at 954 and 925 cm^{-1}. The bands at 825 cm^{-1} in the Raman spectra of the Co-DEG-PMo and Co-TEG-PMo catalysts were assigned to ν(C—O) of TEG (DEG) [51]. Also, there is a band at 973 cm^{-1} that belongs to the characteristic peak of $[PMo_9O_{31}]^{3-}$ or $[PMo_{11}O_{39}]^{7-}$ or $[H_2PMo_{11}O_{39}]^{5-}$ [7–9]. It means that glycols better protect PMo HPA from destruction via the interaction with the alumina support than CA.

3.1.3. Temperature-programmed reduction

TPR-profiles of oxide Co-Add-PMo catalysts are shown in Fig. 1S. The first peak in the 300–550 °C temperature range corresponds to Mo^{6+} reduction to Mo^{4+}, and, probably, to partial Co^{2+} reduction to Co^0. Maximum temperature of 516 °C of the first peak was recorded for the reference Co-PMo sample prepared without any additives. All selected organic additives led to decreasing of the first peak maximum down to ca. 500 °C (for TEG and CA). Complete reduction of all metal particles, including finely dispersed tetrahedral molybdenum and remained cobalt species, took place at 550–1000 °C. All Co-Add-PMo catalysts exhibited a lower temperature of the second reduction peak compared to reference Co-PMo, what witnessed to the weakness of the interaction between metal oxide species and alumina support.

3.1.4. Thermal analysis

The DSC curves for the Co-Add-PMo catalysts (Fig. 2S) show a broad endothermic peak at about 85–100 °C associated with dehydration reactions [52,53], meanwhile the exothermal peaks observed at a temperature lower than 500 °C seemed to emerge due to the decomposition of the Co-Add-PMo complexes. The maximum of water evolution endothermic peak is shifted to a higher temperature for the Co-EG-PMo catalyst compared to the Co-DEG-PMo and Co-TEG-PMo samples, probably, because of a stronger interaction and coordination with adsorbed water.

The exothermic peaks centered in the 240–270 °C range on the DSC curves could be assigned to the initial decomposition (decarboxylation reactions) of Co-Add-PMo and gradual decomposition by heating of chelated metallic species, whereas the exothermic peak at 400–430 °C is mainly attributed to decarboxylation/oxidation reactions of remaining carbonaceous fragments of organic additives. The exothermic peak maximum decreases in the order Co-TEG-PMo > Co-DEG-PMo > Co-EG-PMo. It is supposed that a higher decomposition temperature corresponds to a greater complex stability. The high intensive exothermic peak at 400 °C observed for the Co-Gly-PMo catalyst can be explained by a low tolerance of Co-Gly-PMo complexes. In contrast, the DSC curve of the Co-CA-PMo sample shows very low intensity caused by high stability of such complexes.

3.2. Characteristics of sulfided catalysts

3.2.1. High-resolution transmission electron microscopy

Fig. 5 shows representative HRTEM micrographs of sulfided Co-ADD-PMo catalysts. Morphological characteristics of the active phase species attained by statistical processing of the HRTEM micrographs are summarized in Table 2. The reference Co-PMo catalyst is characterized by a relatively long length and low average stacking number equal to 3.0 nm and 1.45, respectively, which resulted in a lower active phase dispersion (D) compared to that of Co-Add-PMo. The presence of organic additives in the impregnation solution led to a decrease of the average length and an increase of the average stacking number. The lowest average length

Table 2
Morphological characteristics of the CoMoS phase species calculated from TEM micrographs.

Catalyst	Average length $\bar{L}$ (nm)	Average stacking number N	Dispersion of CoMoS D [a]	Distribution of slab length (rel.%)						Distribution of stacking number (rel.%)			
				<2 nm	2–4 nm	4–6 nm	6–8 nm	8–10 nm	>10 nm	1	2	3	>4
Co-PMo	3.00	1.45	0.38	38	44	8	5	2	3	63	31	5	1
Co-CA-PMo	2.75	1.72	0.41	43	40	7	8	1	1	47	39	11	3
Co-EG-PMo	2.81	1.53	0.40	40	45	6	5	2	2	60	31	7	2
Co-DEG-PMo	2.55	1.57	0.44	45	43	6	3	2	1	58	32	8	2
Co-TEG-PMo	2.70	1.83	0.42	43	41	8	5	2	1	44	38	14	4
Co-Gly-PMo	2.73	1.63	0.41	42	43	8	3	2	2	55	34	8	3
Co-EG-CA-PMo	2.75	1.70	0.41	40	44	9	4	2	1	48	38	12	2

[a] CoMoS dispersion calculated from HRTEM results (Eq. (7)).

Table 3
Metal fractions measured by XPS for cobalt and molybdenum species present at the surface of sulfided Co-Add-PMo catalysts.

Catalyst	Co percentage (%)			Mo percentage (%)			Mo/Al	Co/Al	$\left(\frac{Co}{Mo}\right)_{slab}$ [a]	$\left(\frac{Co}{Mo}\right)_{edge}$ [b]	$\left(\frac{S}{Co+Mo}\right)$	Number of Mo^{IV}_{edge} sites (10^{20} at g^{-1})
	CoMoS	CoS_x	Co^{2+}	MoS_2	MoS_xO_y	Mo^{6+}						
Co-PMo	18	47	35	70	12	18	0.076	0.032	0.11	0.29	1.70	1.46
Co-CA-PMo	63	18	20	76	14	10	0.091	0.042	0.38	0.92	1.76	1.77
Co-EG-PMo	25	61	14	75	15	10	0.093	0.038	0.13	0.33	1.75	1.76
Co-DEG-PMo	65	15	20	77	13	10	0.103	0.040	0.33	0.75	1.74	1.81
Co-TEG-PMo	64	13	24	78	13	9	0.123	0.051	0.34	0.81	1.81	2.17
Co-Gly-PMo	53	27	19	78	14	8	0.097	0.037	0.26	0.63	1.75	1.75
Co-EG-CA-PMo	59	18	23	77	14	9	0.108	0.045	0.32	0.78	1.78	1.79

[a] Co/Mo ratio in the CoMoS slabs calculated from XPS results (Eq. (3)).
[b] Co/Mo ratio in the CoMoS edges calculated from XPS and HRTEM results (Eq. (4)).

Table 4
Catalytic properties of prepared Co-Add-PMo catalysts in DBT HDS.

Catalyst	DBT conversion (%) at LHSV		Selectivity ratio S_{HYD}/S_{DDS} at LHSV		Rate constant $\times 10^4$ (mol h^{-1} g^{-1}) k_{HDS}	Turnover frequency TOF_{edge} values $\times 10^4$ (s^{-1})
	80 h^{-1}	40 h^{-1}	80 h^{-1}	40 h^{-1}		
Co-PMo	11.9	22.9	0.032	0.035	9.3 ± 0.1	9.5 ± 0.2
Co-CA-PMo	17.8	32.7	0.081	0.102	16.8 ± 0.1	13.8 ± 0.3
Co-EG-PMo	14.2	27.0	0.072	0.086	11.7 ± 0.1	10.0 ± 0.2
Co-DEG-PMo	16.7	29.1	0.070	0.082	13.4 ± 0.2	10.9 ± 0.2
Co-TEG-PMo	19.5	35.8	0.096	0.101	17.9 ± 0.2	11.8 ± 0.2
Co-Gly-PMo	15.9	29.1	0.040	0.052	13.5 ± 0.1	11.4 ± 0.2
Co-EG-CA-PMo	15.7	29.7	0.068	0.069	15.6 ± 0.2	12.8 ± 0.2

Conditions: T = 250 °C, P = 3.0 MPa, H_2/HC = 500 NL/L.

of 2.55 nm was determined for the Co-DEG-PMo catalyst; other studied additives decreased the average length to ca. 2.8 nm. The maximum average stacking number equal to of 1.83 was found for the Co-TEG-PMo catalyst. The Co-DEG-PMo sample exhibited a higher dispersion among the active phase species (0.44) and had the minimal average length.

3.2.2. XPS spectroscopy

The chemical surface composition of sulfided catalysts was evaluated by XPS. The Co 2p and Mo 3d XPS spectra of sulfided Co-Add-PMo catalysts are shown in Figs. 6 and 3S , respectively. The spectral region of Co $2p_{3/2}$ (Fig. 6) contains three peaks with their respective satellites. The peak at BE of 778.6 eV is related to Co in the CoMoS phase species. The signals at 778.1 and 781.5 eV correspond to the CoS_x species and to Co^{2+} in an oxidic environment, respectively [37,38,42,54]. The Mo 3d spectra (Fig. 3S) contain three Mo 3d doublets, namely [37,38,42,54]: (1) the Mo $3d_{5/2}$ and $3d_{3/2}$ doublet with BE at 228.8 and 232.0 eV, respectively, corresponds to the Mo^{4+} in MoS_2 phase species, (2) the doublet with BE equal to 230.0 and 233.2 eV is related to Mo^{5+} in the MoS_xO_y oxysulfide species, and (3) finally, the doublet at 232.1 and 235.3 eV belongs to the Mo^{6+} oxide species. The peak at BE of 226.1 eV is assigned to S 2s.

The decomposition of the recorded XPS spectra (Figs. 6 and 3S) allowed estimating the chemical surface composition of the prepared Co-Add-PMo catalysts. The results of the XPS spectra decomposition are summarized in Table 3. The reference Co-PMo catalyst characterized by a lower sulfidation degree had the lowest percentage of cobalt in the CoMoS phase (18 rel.%) and molybdenum in MoS_2 particles (70 rel.%), consequently, the highest of amounts of Co and Mo oxides were present on the catalysts surface. The organic additives induced the increase of the S/(Co + Mo) ratio from 1.70 to 1.81 and the cobalt amount in CoMoS species. The Co and Mo percentage in the oxidic sate dropped from 35 to 14 rel.% and from 18 to 8 rel.%, respectively. The cobalt percentage maximum of ca. 65 rel.% in the CoMoS phase was found for Co-CA-PMo, Co-DEG-PMo and Co-TEG-PMo catalysts. The presence of organic additives in the impregnation solution was favorable both for the Co and Mo dispersion on the catalyst surface and for the promotion degree of the CoMoS active phase. The $(Co/Mo)_{slab}$ ratio increased from 0.11 (reference Co-PMo sample) to 0.38 (Co-CA-PMo catalyst), meanwhile the $(Co/Mo)_{edge}$ ratio rose from 0.29 to 0.92 for the same catalysts. The use of organic additives resulted

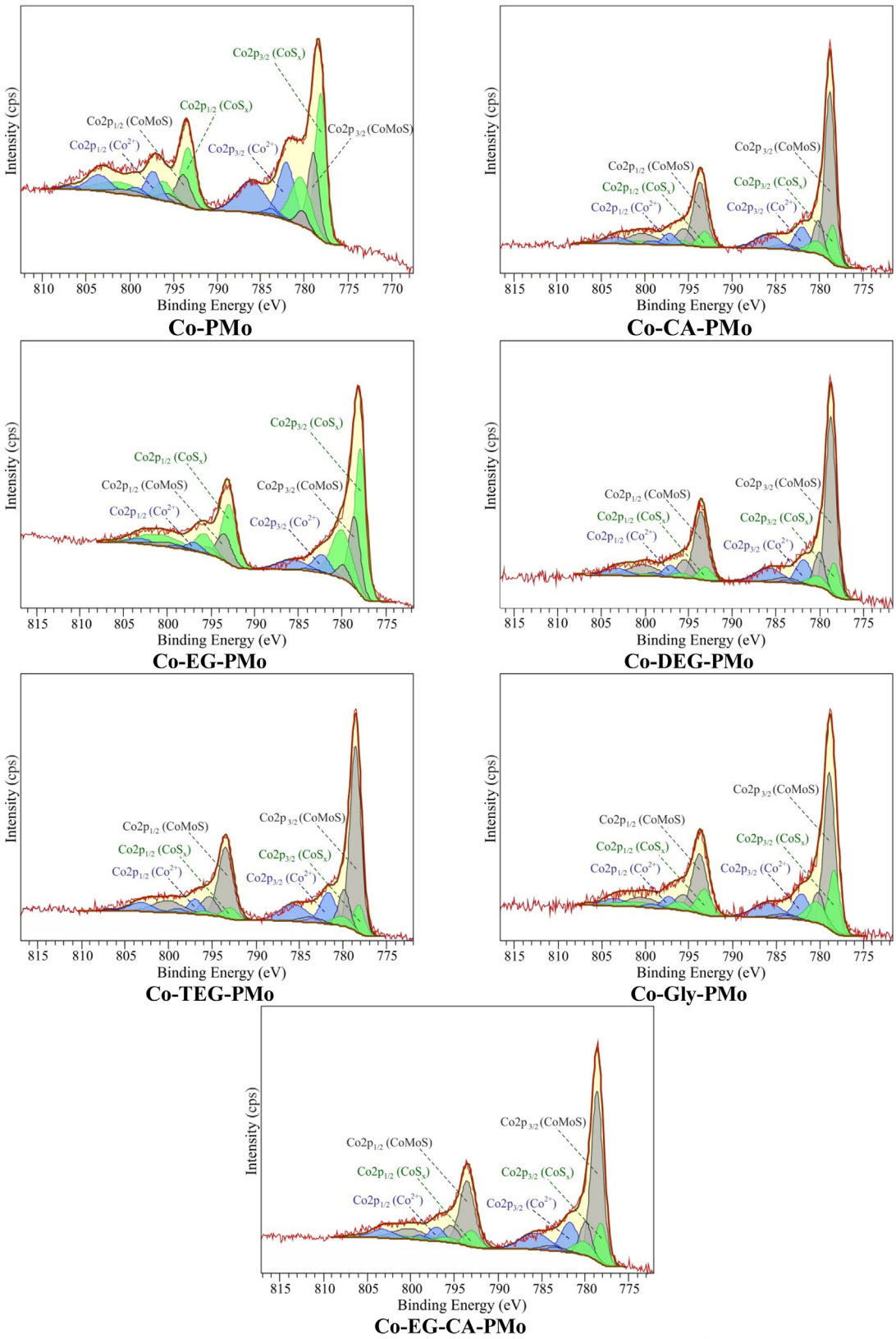

Fig. 4. XPS Co 2p spectra of sulfided Co-Add-PMo catalysts; in blue: Co^{2+} oxide contributions; in green: CoS_x contributions; in grey: CoMoS phase contributions. (For interpretation of the references to color in this figure legend, the reader is referred to the web version of the article).

in the increased number of Mo^{IV}_{edge} sites from 1.46×10^{20} at g^{-1} in the Co-PMo catalyst to 2.17×10^{20} at g^{-1} for the Co-TEG-PMo sample.

3.2.3. Temperature-programmed reduction of sulfided catalysts

Fig. 5 shows the TPR curves of sulfided catalysts. The peak observed at 200–340 °C corresponds to the reduction of sulfur

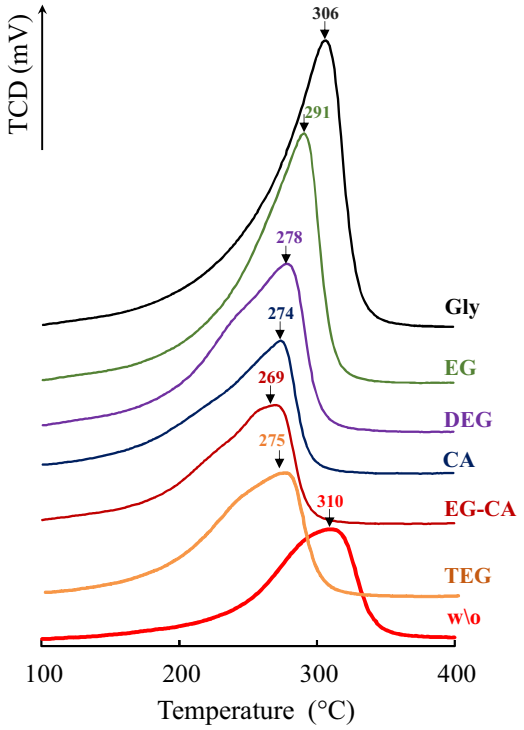

Fig. 5. TPR curves for sulfided Co-Add-PMo catalysts.

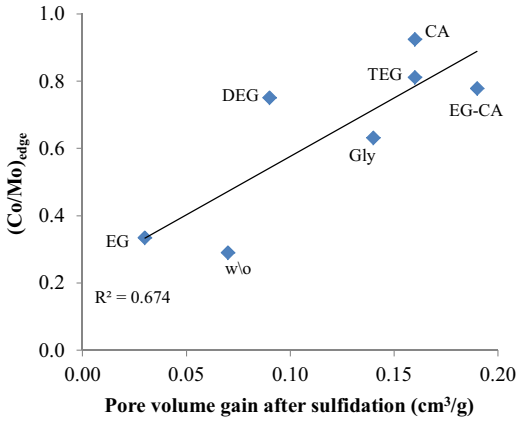

Fig. 6. Promotion degree of CoMoS edges vs catalyst pore volume gain after sulfidation.

atoms from the edges of MoS_2-based active phase slabs [55,56]. The temperature maximum of the first reduction peak depends on the organic additive type used in the impregnation solution. The first peak temperature is considered to be indicative of the Mo-S bond strength [55]. Each TPR curve has a shoulder at low temperature that related to reduction of more reactive M-S sites (or S_2^{2-}) due to nonuniform centre distribution into CoMoS slabs (M- and S-edges, mixed sites, etc.) as well as the presence of particles with different size and morphology [2,3,36,37,56]. The reference sample prepared without any additive exhibited higher reduction peak temperature of 310 °C. All tested additives brought about the reduction peak temperature decrease in the following order: Gly > EG > DEG > CA ≈ TEG > EG-CA. The lowest temperature equal to ca. 269 °C with a wide shoulder to lower temperature was observed for the Co-EG-CA-PMo catalyst, which means that such catalyst possesses more labile sulfur atoms and, consequently, more reactive active sites.

3.3. Catalytic activity in DBT hydrodesulfurization

In this study, catalytic activity of Co-Add-PMo catalysts was evaluated in the DBT HDS reaction. This molecule was selected as the most representative sulfur-containing compound present in oil-derived middle distillates [3]. Table 4 shows catalytic properties of the prepared catalysts in DBT HDS. The steady state DBT conversion over the catalysts varied from 11.9 to 35.8% depending on the sample and LHSV chosen. The Co-PMo catalyst demonstrated lower activity in DBT HDS (the rate constant was 9.3×10^4 mol h^{-1} g^{-1}). The additive-containing catalysts demonstrated higher DBT conversion at both residence times compared to the reference Co-PMo analog. The Co-TEG-PMo and Co-CA-PMo samples had the highest HDS rate constants equal to 17.9×10^4 and 16.8×10^4 mol h^{-1} g^{-1}, respectively. Selectivity ratio $S_{HYD}/_{DDS}$ values varied from 0.032 to 0.102 that is in agreement with the known HDS mechanism of the DBT molecule and the direct desulfurization pathway predominating over the pre-hydrogenation one. Maximal $S_{HYD}/_{DDS}$ (ca. 0.101) corresponded to the most active samples and vice versa.

4. Discussion

4.1. Comparison of citric acid and glycol effects on the state of the CoMoS species

It is well known that $CoMo/Al_2O_3$ catalyst performance improves by adding chelating or complexing agents to the impregnating solution. The role of chelating agents was explained by the optimization of CoMoS phase formation due to the following mechanisms: (i) a decrease of the Co partition in the $CoAl_2O_4$ phase [2,3,57]; (ii) optimization of sulfidation rates of Co and Mo species [37–39,42,57–63]; (iii) an improvement of the Mo and/or Co dispersion [2,9,39,61–63]; (iv) a reduction of the interaction between loading metals and the support [37,39,57,63–67]. The use of chelating agents has led to a new generation of industrial HDT catalysts.

Later on, organic additives such as glycols and polyols were proposed to improve HDS catalysts. Iwamoto et al. [68] investigated the addition of polyethylene glycol (PEG) as a water-soluble organic compound to the impregnation solution during catalyst preparation to improve $NiO\text{-}MoO_3/Al_2O_3$ and $NiO\text{-}MoO_3\text{-}P_2O_5/Al_2O_3$ HDS catalysts. XPS measurements suggested that the PEG addition increased the nickel and molybdenum dispersion on the alumina support and improved DBT and atmospheric residue HDS activity. The authors concluded that PEG might block the aggregation of active metal precursors in the drying step and increase the number of HDS sites. A similar effect was later discovered for EG as an organic additive. Escobar et al. [69], using digestion of MoO_3 in the H_3PO_4 preparation method, demonstrated by TPR that the interaction between alumina and the active phase species decreased in the presence of EG and that the dispersion depended on the EG/Mo ratio. Nicosia and Prins [51] have shown another role of an organic additive. They reported that, by decreasing the surface area and pore volume of the γ-Al_2O_3, TEG favors polyphosphate formation. The structure of cobalt-diphosphopentamolybdate is not retained but is converted to the $PMo_{12}O_{40}^{3-}$ polymolybdate species which can be bound to the promoter atoms. During sulfidation, this may lead to a better decoration of the promoter on terminal MoS_2 slabs, thus explaining the improvement in catalytic performance of the catalysts.

The changes in the beneficial role of glycols can be related to the differences in the nature of precursors used for catalyst preparation. By this reason, Geantet with co-workers carried out a series of several comprehensive studies to elucidate the TEG role in improving HDS catalysts prepared with different Mo pre-

cursors [11,36,70]. Several impregnation solutions that contained ammonium heptamolybdate or cobaltomolybdate heteropolyanions ($CoMo_6O_{24}H_7^{3-}$ and its dimeric form $Co_2Mo_{10}O_{38}H_4^{6-}$) were used for $CoMo/Al_2O_3$ catalysts and the phosphomolybdate heteropolyanion with different P/Mo molar ratios (0.11, 0.40 and 0.57) for $CoMoP/Al_2O_3$ ones. As compared to chelating agents, the TEG effect was not related to complexation but could be attributed to the partial redissolution/redispersion of the active species and the formation of HPA entities with different structures [70]. This redistribution of active species as HPA species gives rise to a catalyst more resistant towards sulfidation. As illustrated by both in situ Raman and X-ray absorption spectroscopy methods, the activation of the $CoMo/Al_2O_3$ catalysts was delayed where TEG had been impregnated on the catalysts. This inhibition occurs at low temperatures (below 473 K). It strongly affects the low temperature exchange between S and O stages and further formation of bridging sulfur pairs. As a consequence, this retardation effect was beneficial for decorated CoMoS active phase formation as evidenced by a more selective catalyst for the DDS route in the 4,6-DMDBT conversion. Similar, although less pronounced observations may be drawn for calcined catalysts.

TPR results revealed that chelating and non-complexing organic additives resulted in reducing the interaction between the metal oxide species and alumina support for all Co-Add-PMo catalysts (Fig. 1S), whatever the nature of the organic additives used. Moreover, a good linear correlation was obtained between the average stacking number of CoMoS slabs and maximum peak reduction for oxide Co-Add-PMo catalysts (Fig. 4S). The weakening of the metal oxide species-support interaction led to growing of the stacking number from 1.45 for the additive-free Co-PMo catalyst to 1.83 for the Co-TEG-PMo one. Indeed, using Raman spectroscopy (Fig. 2), a presence of Al-O-Mo bands was observed for Co-PMo catalysts, which witnessed in favor of a strong interaction of the Mo oxide species with Al_2O_3. In contrast, all additive-containing Co-Add-PMo samples did not have this signal and Raman spectra corresponded to the Mo-containing polyoxometallate species. Previously, N.-Y. Topsøe and H. Topsøe [71] had concluded that surface OH groups in alumina were responsible for formation of unfavorable Al-O-Mo linkages. In this case, the role of citric acid and glycols may consist in lowering the number of OH groups available for interacting with Mo atoms during CoMoS phase formation and thus weakening the interaction of the active phase species with Al_2O_3. Weckhuysen with co-workers [66] previously reported significant effect of CA on Co^{2+} distribution inside Co/Al_2O_3 extrudates due to complex formation and competitive adsorption of free CA molecules. Recently, Escobar et al. [65] reported that impregnating CA on bare alumina carrier prior to Ni-Mo-P deposition resulted in the formation of a catalyst with higher benzothiophene HDS activity than solid obtained via simultaneous Ni-Mo-P-CA deposition. Authors concluded that beneficial "passivation" from citric adsorption/decomposition on the Al_2O_3 support led to weak interaction between Mo and Ni species with the support. On the other hand, the organic additives are reduced during sulfidation with formation of carbon-contained byproducts, which may be directly involved in the lowering of the slab-support interaction [72] or play a role of secondary supports for the catalysts [73] (Fig. 1). Reduced CoMoS-Al_2O_3 interactions are favorable for the stacking number increase in CoMoS slabs. These results are in agreement with those obtained for CA by Chen et al. [64], Gonzalez-Cortes et al. [45], van Haandel et al. [74], Nikulshin and co-workers [37,38,41], and Wu et al. [75] as well as for EG [69] and for TEG reported previously [36,70]. Here, it is demonstrated that the TEG addition let afford less coke and a smaller micropore volume (Table 1) compared to the CA-contained samples, whereas stacking numbers of the formed CoMoS species were close to each other.

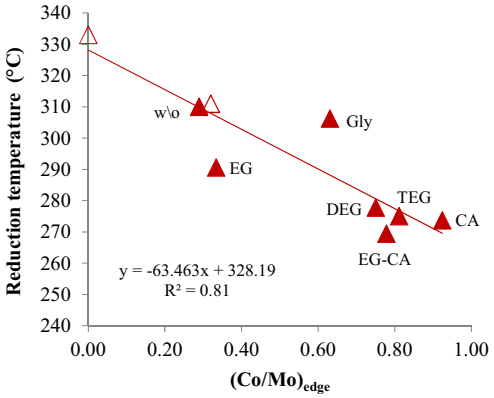

Fig. 7. Dependence of the TPR peak maximum for sulfided Co-Add-PMo catalysts (filled symbols) as well as Mo/Al_2O_3 and $CoMo_6/Al_2O_3$ samples [73] from the promotion degree of CoMoS edges.

The CoMoS slab lengths slightly decreased after introducing organic additives into the catalysts (Table 2), which was related to the increase of the Co partition in the CoMoS species and of the $(Co/Mo)_{edge}$ ratio. The CoMoS size decrease with the simultaneous increase in its promotion degree indicated that Co atoms prevented growth of the slabs during sulfidation by fixing on the edges of MoS_2 formed. The use of Co-CA complexes for catalyst preparation resulted in the increased Co partition in the CoMoS species from 18 to 63 rel.% as well as in the increased edge decoration from 0.29 to 0.92. It is possible due to the known retarding effect of premature sulfidation of Co atoms owing to the existence of the stable Co-CA complex [37–39,42,62,63]. However, using of non-complexing glycols also led to an enhanced yield of the CoMoS species. It is well known that, during liquid phase sulfidation, H_2S molecules are formed from DMDS at a high temperature (200 °C and more). The use of organic additives on the catalyst surface may delay H_2S formation and, subsequently, optimize Co and Mo sulfidation rates. The mechanism of delaying sulfidation for glycols obviously differs from that for chelating agents. Glycols could not form any complexes with promoter atoms although their presence on the catalyst surface and a significant blocking effect, evidencing to a dramatic drop in the SSA and pore volume, may optimize Co and Mo sulfidation rates. Indeed, the DTA analysis has revealed that all tested organic additives started to decompose at ca. 200 °C or above, i.e. the decomposition of blocking agents and metal sulfidation processes occur simultaneously. Moreover, it was found that the promotion degree of CoMoS edges $(Co/Mo)_{edge}$ increased with a pore volume gain by the additive-impregnated catalysts after their sulfidation (Fig. 6). This finding explains why different non-complexing organic additives may delay sulfidation of promoter atoms and enhance CoMoS phase formation.

4.2. Relationships between the composition and morphology of the CoMoS species and its performance

The changes observed in the morphology and composition of CoMoS slabs had an impact on the reduction of sulfided catalysts. Fig. 7 shows the dependence of the TPR peak maximum for sulfided Co-Add-PMo catalysts as well as for the Mo/Al_2O_3 and $CoMo_6/Al_2O_3$ samples reported previously [76] on the promotion degree of CoMoS edges $(Co/Mo)_{edge}$. It is clear that the organic additives led to several beneficial effects such as weakening of the slab-support interaction at enhancing the CoMoS species promotion degree and stacking number. All these changes resulted in decreasing the temperature of maximum peak reduction for sulfided Co-Add-PMo catalysts due to formation of more reactive mixed Co-Mo sites. Another possible transformation should

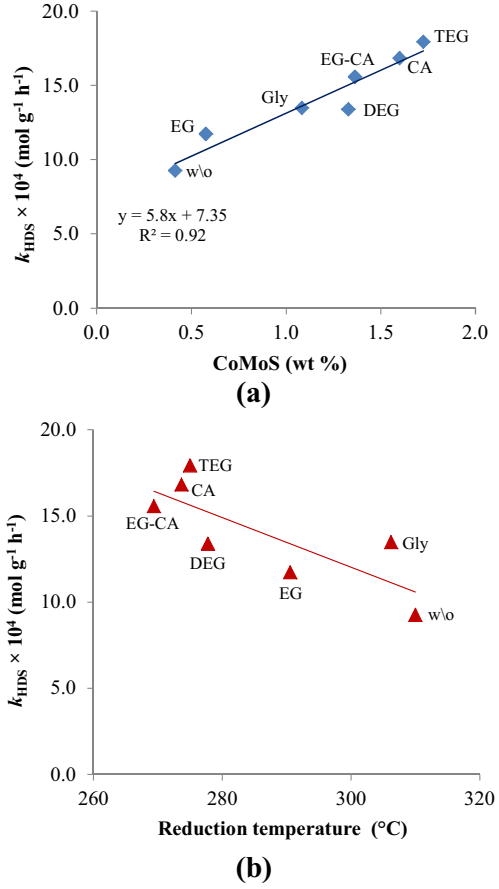

Fig. 8. Dependence of rate constants in DBT HDS from the effective Co amount in the CoMoS phase species **(a)** and maximum peak reduction temperature **(b)** for sulfided Co-Add-PMo catalysts.

also be considered. Using low-temperature CO adsorption followed by the IR spectroscopy characterization Mauge with co-workers have established [64] that the CA addition during preparation of MoS_2/Al_2O_3 catalysts promotes growth of the S-edge at the expense of the M-edge on the MoS_2 slab. By varying the amount of CA additives, it was demonstrated that the morphology of MoS_2 slab on Al_2O_3 could be progressively modified from a slightly truncated triangle with the M-edge predominant to the hexagon with both the M-edge and S-edge. Possible mechanisms of the MoS_2 changes were suggested to be the lowering of the slab-support interaction due to the addition of CA molecules that can protect the Mo oxide species from a strong contact with Al-OH groups as well as the coke species formation. Here, we can suggest that the addition of CA and other organic additives used in the study may also increase the S/M edge ratio in MoS_2 slabs during sulfidation, which is favorable for fixing more Co atoms on the S-edges and leading to an excess of CoMoS sites.

HDS activity of all prepared sulfided Co-Add-PMo catalysts linearly increased with the effective Co amount in the CoMoS phase species and decreased from its TPR peak maximum (Fig. 8). An origin of the obtained relationships comes from a linear dependence of the TPR peak maximum from the promotion edge degree $(Co/Mo)_{edge}$ of CoMoS slabs (Fig. 7). The Co-Add-PMo samples with CA, TEG or the EG-CA mixture demonstrated the highest HDS activity. Fig. 9 shows the dependence of the TOF number in DBT HDS normalized on the edge sites of CoMoS slabs over the Co-Add-PMo catalysts on the average length of the CoMoS phase species and $(Co/Mo)_{edge}$ ratio. The TOF number increased with a decrease of the active phase species size and an increase of the promotion degree

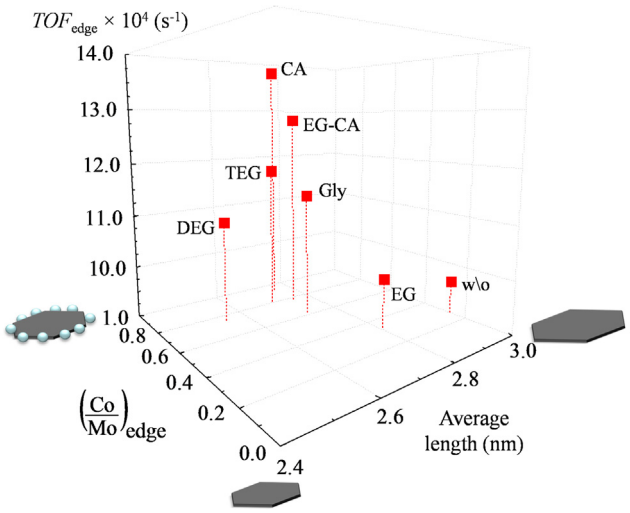

Fig. 9. 3D dependence of the TOF number in DBT HDS over Co-Add-PMo catalysts from the average length of the CoMoS phase species and $(Co/Mo)_{edge}$ ratio.

of $(Co/Mo)_{edge}$. The CA-contained catalyst had the highest TOF_{edge} number owing to the moderate average length of the CoMoS species and its maximal $(Co/Mo)_{edge}$ ratio among all studied catalytic systems.

5. Conclusions

This study investigated differences in the state of the active phase species and catalytic properties of Co-PMo/Al_2O_3 HDS catalysts prepared from Keggin-type HPA and Co complexes with CA or non-complexing organic additives (EG, TEG and Gly). It has been found that the addition of either CA or glycols led to several beneficial effects such as weakening of the slab-support interaction at enhancing the CoMoS species promotion degree, dispersion and stacking number.

The length of CoMoS slabs slightly decreased after introducing organic additives into the catalysts, which is related to the increase of the Co partition in the CoMoS phase species and the $(Co/Mo)_{edge}$ ratio. The CoMoS size decrease at the simultaneous increase of its promotion degree indicated that Co atoms prevented growth of the slabs during sulfidation by fixing on the edges of MoS_2 formed. All the changes resulted in decreasing the TPR peak maximum for sulfided Co-Add-PMo catalysts due to formation of more reactive mixed Co-Mo sites. It has been shown that the promotion degree of the CoMoS edges increased with a pore volume gain by the additive-impregnated catalysts after their sulfidation. It was supposed that non-complexing organic additives on the catalyst surface might delay H_2S formation from DMDS and, subsequently, optimize Co and Mo sulfidation rates.

It has been shown that glycols provide better protection of PMo HPA against destruction via the interaction with the alumina support than CA. The TEG addition allows less coke and a smaller micropore volume compared to the CA-contained samples, whereas the promotion degree and stacking number of the formed CoMoS species are close in value.

The Co-Add-PMo samples with CA, TEG or the EG-CA mixture demonstrated the highest activity in DBT HDS. The TOF number increased with the decrease of the active phase species size and the increase of promotion degree of $(Co/Mo)_{edge}$. The CA-contained catalyst had the highest TOF_{edge} number owing to the moderate average length of the CoMoS species and its maximal $(Co/Mo)_{edge}$ ratio among all tested catalytic systems.

Acknowledgments

The study was supported by Ministry of Education and Science of the Russian Federation, project No 14.577.21.0173 (Unique identifier of applied scientific researches and experimental developments (project number) RFMEFI57715X0173).

Appendix A. Supplementary data

Supplementary data associated with this article can be found, in the online version, at http://dx.doi.org/10.1016/j.apcatb.2016.12.022.

References

[1] L. He, F. Lin, X. Li, H. Sui, Z. Xu, Chem. Soc. Rev. 44 (2015) 5446–5494.
[2] H. Topsøe, B.S. Clausen, F.E. Massoth, in: J.R. Anderson, M. Boudart (Eds.), Hydrotreating Catalysis-Science and Technology, Springer-Verlag, Berlin-Heidelberg, NY, 1996, p. 310.
[3] Catalysis by transition metal sulphides, in: H. Toulhoat, P. Raybaud (Eds.), From Molecular Theory to Industrial Applications, Technip Edition, Paris, 2013, p. 832.
[4] P. Nikulshin, A. Mozhaev, C. Lancelot, P. Blanchard, E. Payen, C. Lamonier, C. R. Chimie 19 (10) (2016) 1276.
[5] A. Spozhakina, B. Gigov, D. Shokov, React. Kinet. Catal. Lett. 19 (1–2) (1982) 11.
[6] A. Spozhakina, S. Damyanova, V. Sharkova, D. Shokov, T. Yureva, Proceedings of 6th International Symposium on Hererogeneous Catalysis, Sofia, 1987, p. 503.
[7] A. Griboval, P. Blanchard, E. Payen, M. Fournier, J.L. Dubois, Catal. Today 45 (1998) 283.
[8] A. Griboval, P. Blanchard, E. Payen, M. Fournier, J.L. Dubois, J.R. Bernard, Appl. Catal. A 217 (2001) 173.
[9] J.A. Bergwerff, L.G.A. Van De Water, T. Visser, P. De Peinder, B.R.G. Leliveld, K.P. De Jong, B.M. Weckhuysen, Chem. Eur. J. 11 (2005) 4591.
[10] N.N. Tomina, P.A. Nikul'shin, A.A. Pimerzin, Pet. Chem. 48 (2) (2008) 92.
[11] V. Costa, K. Marchand, M. Digne, C. Geantet, Catal. Today 130 (2008) 69.
[12] K. Ben Tayeb, C. Lamonier, C. Lancelot, M. Fournier, E. Payen, A. Bonduelle, F. Bertoncini, Catal. Today 150 (2010) 207.
[13] D. Soogund, B. Guichard, A. Daudin, C. Lamonier, E. Payen, Appl. Catal. B 98 (2010) 39.
[14] A. Romero-Galarza, A. Gutiérrez-Alejandre, J. Ramírez, J. Catal. 280 (2011) 230.
[15] A.A. Pimerzin, N.N. Tomina, P.A. Nikul'shin, N.M. Maksimov, A.V. Mozhaev, D.I. Ishutenko, E.E. Vishnevskaya, Catal. Ind. 7 (1) (2015) 30.
[16] A.M. Maitra, N.W. Cant, D.L. Trimm, Appl. Catal. 48 (1989) 187.
[17] C.I. Cabello, I.L. Botto, H.J. Thomas, Appl. Catal. A 197 (2000) 79.
[18] C.I. Cabello, M. Munoz, E. Payen, H.J. Thomas, Catal. Lett. 92 (1–2) (2004) 69.
[19] C. Martin, C. Lamonier, M. Fournier, O. Mentré, V. Harlé, D. Guillaume, E. Payen, Chem. Mater. 17 (2005) 4438.
[20] P.A. Nikul'shin, Y.V. Eremina, N.N. Tomina, A.A. Pimerzin, Pet. Chem. 46 (5) (2006) 343.
[21] C.I. Cabello, M. Munoz, I.L. Botto, E. Payen, Thermochim. Acta 447 (2006) 22.
[22] M. Munoz, C.I. Cabello, I.L. Botto, G. Minelli, M. Capron, C. Lamonier, E. Payen, J. Mol. Struct. 841 (2007) 96.
[23] C. Lamonier, C. Martin, J. Mazurelle, V. Harlé, D. Guillaume, E. Payen, Appl. Catal. B 70 (2007) 548.
[24] N.N. Tomina, P.A. Nikul'shin, A.A. Pimerzin, Kinet. Catal. 49 (5) (2008) 653.
[25] P.A. Nikul'shin, N.N. Tomina, Y.V. Eremina, A.A. Pimerzin, Russ. J. Appl. Chem. 82 (1) (2009) 86.
[26] N.N. Tomina, P.A. Nikul'shin, V.S. Tsvetkov, A.A. Pimerzin, Kinet. Catal. 50 (2) (2009) 220.
[27] P.A. Nikulshin, N.N. Tomina, A.A. Pimerzin, A.V. Kucherov, V.M. Kogan, Catal. Today 149 (1–2) (2010) 82.
[28] R. Palcheva, A. Spojakina, K. Jiratova, L. Kaluza, Catal. Lett. 137 (2010) 216.
[29] P.A. Nikulshin, N.N. Tomina, A.A. Pimerzin, A. Yu Stakheev, I.S. Mashkovsky, V.M. Kogan, Appl. Catal. A 393 (2011) 146.
[30] P.A. Nikul'shin, A.V. Mozhaev, D.I. Ishutenko, P.P. Minaev, A.I. Lyashenko, A.A. Pimerzin, Kinet. Catal. 53 (5) (2012) 620.
[31] L. Kaluža, R. Palcheva, A. Spojakina, K. Jirátová, G. Tyuliev, Proc. Eng. 42 (2012) 873.
[32] P. Blanchard, C. Lamonier, A. Griboval, E. Payen, Appl. Catal. A 322 (2007) 33.
[33] J. Liang, Y. Liu, J. Zhao, X. Li, Y. Lu, M. Wu, C. Liu, Catal. Lett. 144 (2014) 1735.
[34] C.I. Cabello, F.M. Cabrerizo, A. Alvarez, H.J. Thomas, J. Mol. Catal. A: Chem. 186 (2002) 89.
[35] P.A. Nikul'shin, A.V. Mozhaev, A.A. Pimerzin, N.N. Tomina, V.V. Konovalov, V.M. Kogan, Kinet. Catal. 52 (6) (2011) 862.
[36] V. Costa, B. Guichard, M. Digne, C. Legens, P. Lecour, K. Marchand, P. Raybaud, E. Krebs, C. Geantet, Catal. Sci. Technol. 3 (2013) 140.
[37] P.A. Nikulshin, D.I. Ishutenko, A.A. Mozhaev, K.I. Maslakov, A.A. Pimerzin, J. Catal. 312 (2014) 152.
[38] A.V. Mozhaev, P.A. Nikulshin, Al.A. Pimerzin, K.I. Maslakov, A.A. Pimerzin, Catal. Today 271 (2016) 80.
[39] J. Ramírez, A. Gutieírrez-Alejandre, F. Saínchez-Minero, V. Macías-Alcaíntara, P. Castillo-Villaloín, L. Oliviero, F. Maugeí, Energy Fuels 26 (2012) 773.
[40] P.P. Minaev, P.A. Nikulshin, M.S. Kulikova, A.A. Pimerzina, V.M. Kogan, Appl. Catal. A 505 (2015) 456.
[41] P.A. Nikulshin, P.P. Minaev, A.V. Mozhaev, K.I. Maslakov, M.S. Kulikova, A.A. Pimerzin, Appl. Catal. B 176 (2015) 374.
[42] P.A. Nikulshin, A.V. Mozhaev, K.I. Maslakov, A.A. Pimerzin, V.M. Kogan, Appl. Catal. B 158–159 (2014) 161.
[43] S. Kasztelan, H. Toulhoat, J. Grimblot, J.P. Bonnelle, Appl. Catal. 13 (1984) 127.
[44] G. Berhault, M. Perez De la Rosa, A. Mehta, M.J. Yácaman, R.R. Chianelli, Appl. Catal. A 345 (2008) 80.
[45] S.L. Gonzalez-Cortes, Y. Qian, H.A. Almegren, T. Xiao, V.L. Kuznetsov, P.P. Edwards, Appl. Petrochem. Res. 5 (2015) 181.
[46] J.A. Bergwerff, T. Visser, B.M. Weckhuysen, Catal. Today 130 (2008) 117–125.
[47] G. Mestl, T.K.K. Srinivasan, Catal. Rev. Sci. Eng. 40 (1998) 451–570.
[48] J.A. Bergwerff, T. Visser, B.R.G. Leliveld, B.D. Rossenaar, K.P. de Jong, B.M. Weckhuysen, J. Am. Chem. Soc. 126 (2004) 14548–14556.
[49] C. Martin, C. Lamonier, M. Fournier, O. Mentré, V. Harlé, D. Guillaume, E. Payen, Inorg. Chem. 43 (2004) 4636–4644.
[50] J.A. Bergwerff, M. Jansen, B.R.G. Leliveld, T. Visser, K.P. de Jong, B.M. Weckhuysen, J. Catal. 243 (2006) 292–302.
[51] D. Nicosia, R. Prins, J. Catal. 234 (2005) 414–420.
[52] J. De Boer, J.M.H. Fortuin, B.C. Lippens, W.H. Meijs, J. Catal. 2 (1963) 1–7.
[53] S. Gonzaílez-Corteís, T. Xiao, P.M.F.J. Costa, B. Fontal, M.L.H. Green, Appl. Catal. A 270 (2004) 209–222.
[54] A.D. Gandubert, E. Krebs, C. Legens, D. Costa, D. Guillaume, P. Raybaud, Catal. Today 130 (2008) 149–159.
[55] B. Scheffer, N.J.J. Dekker, P.J. Mangnus, J.A. Moulijn, J. Catal. 121 (1990) 31–46.
[56] N. Dinter, M. Rusanen, P. Raybaud, S. Kasztelan, P. da Silva, H. Toulhoat, J. Catal. 275 (2010) 117–128.
[57] M. Breysse, C. Geantet, P. Afanasiev, J. Blanchard, M. Vrinat, Catal. Today 130 (2008) 3–13.
[58] L. Coulier, V.H.J. de Beer, J.A.R. van Veen, J.W. Niemantsverdriet, J. Catal. 197 (2001) 26.
[59] G. Kishan, L. Coulier, J.A.R. van Veen, J.W. Niemantsverdriet, J. Catal. 200 (2001) 194.
[60] R. Cattaneo, Th. Weber, T. Shido, R. Prins, J. Catal. 191 (2000) 225.
[61] N. Frizi, P. Blanchard, E. Payen, P. Baranek, C. Lancelot, M. Rebeilleau, C. Dupuy, J.P. Dath, Catal. Today 130 (2008) 32–40.
[62] T.E. Klimova, D. Valencia, J.A. Mendoza-Nieto, P. Hernández-Hipólito, J. Catal. 304 (2013) 29–46.
[63] A.V. Pashigreva, G.A. Bukhtiyarova, O.V. Klimov, Y.A. Chesalov, G.S. Litvak, A.S. Noskov, Catal. Today 149 (2010) 19–27.
[64] J. Chen, F. Maugé, J. El Fallah, L. Oliviero, J. Catal. 320 (2014) 170–179.
[65] J. Escobar, M.C. Barrera, A.W. Gutiérrez, J.E. Terrazas, Fuel Process. Technol. 156 (2017) 33–42.
[66] J.A. Bergwerff, A.A. Lysova, L. Espinosa-Alonso, I.V. Koptyug, B.M. Weckhuysen, Chem. Eur. J. 14 (2008) 2363–2374.
[67] L.G.A. van de Water, J.A. Bergwerff, B.G. Leliveld, B.M. Weckhuysen, K.P. de Jong, J. Phys. Chem. B 109 (2005) 14513–14522.
[68] R. Iwamoto, N. Kagami, Y. Sakoda, A. Iino, J. Jpn. Petrol. Inst. 48 (2005) 351–357.
[69] J. Escobar, M.C. Barrera, J.A. Toledo, M.A. Cortes-Jacome, C. Angeles-Chavez, S. Nunez, V. Santes, E. Gomez, L. Diaz, E. Romero, J.G. Pacheco, Appl. Catal. B 88 (2009) 564–575.
[70] T.S. Nguyen, S. Loridant, L. Chantal, T. Cholley, C. Geantet, Appl. Catal. B 107 (2011) 59–67.
[71] N.Y. Topsøe, H. Topsøe, J. Catal. 139 (1993) 631–640.
[72] C. Glasson, C. Geantet, M. Lacroix, F. Labruyere, P. Dufresne, J. Catal. 212 (2002) 76–85.
[73] N. Rinaldi, T. Kubota, Y. Okamoto, Ind. Eng. Chem. Res. 48 (2009) 10414–10424.
[74] L. van Haandel, G.M. Bremmer, E.J.M. Hensen, T. Weber, J. Catal. 342 (2016) 27–39.
[75] H. Wu, A. Duan, Z. Zhao, D. Qi, J. Li, B. Liu, G. Jiang, J. Liu, Y. Wei, X. Zhang, Fuel 130 (2014) 203–210.
[76] D. Ishutenko, A. Mozhaev, V. Salnikov, P. Nikulshin, React. Kinet. Mech. Catal. 119 (2016) 615.